International Journal of Heat and Mass Transfer 117 (2018) 1291–1303

Contents lists available at ScienceDirect

International Journal of Heat and Mass Transfer

journal homepage: www.elsevier.com/locate/ijhmt

Forced convection of nanofluids in an extended surfaces channel using lattice Boltzmann method

Rasul Mohebbi [a,*], M.M. Rashidi [b], Mohsen Izadi [c], Nor Azwadi Che Sidik [d,e,*], Hong Wei Xian [e]

[a] School of Engineering, Damghan University, Damghan, Iran
[b] Department of Civil Engineering, School of Engineering, University of Birmingham, Birmingham, UK
[c] Mechanical Engineering Department, Faculty of Engineering, Lorestan University, Khorramabad, Iran
[d] Faculty of Mechanical Engineering, Universiti Teknologi Malaysia, 81310 UTM Skudai, Johor, Malaysia
[e] Malaysia – Japan International Institute of Technology (MJIIT), University Teknologi Malaysia Kuala Lumpur, Jalan Sultan Yahya Petra (Jalan Semarak), 54100 Kuala Lumpur, Malaysia

ARTICLE INFO

Article history:
Received 11 May 2017
Received in revised form 13 October 2017
Accepted 16 October 2017
Available online 5 November 2017

Keywords:
Nanofluid
LBM
Parallel-plate channel
Extended surfaces
Laminar forced convection
Nusselt number

ABSTRACT

Research on nanofluids for heat transfer augmentation has received a great attention from many researchers. Recently, many numerical works have been conducted to examine their applicability in predicting heat transfer with nanofluids. In the present study, a two-dimensional (2D) lattice Boltzmann method (LBM) was applied for numerical simulation of forced convection in a channel with extended surface using three different nanofluids. The predicted were carried out for the laminar nanofluid flow at low Reynolds number ($10 \leqslant Re \leqslant 70$), nanofluid concentration ($0.00 \leqslant \varphi \leqslant 0.050$), different geometric parameter ($0.2 \leqslant A = l/H \leqslant 0.8$) and relative height of the extended surfaces ($0.05 \leqslant B = h/H \leqslant 0.35$). The results indicated that the average Nusselt number increases when the nanofluid concentration increased from 0% to 5%. Moreover, the effect of the nanofluid concentration on the increasing of heat transfer is more noticeable at higher values of the Reynolds number. It is concluded that the use of extended surfaces can enhance the rate of heat transfer for certain arrangements. We also found that the nanofluid with CuO nanoparticles performed better enhancement on heat transfer compared Al_2O_3/water and TiO_2/water nanofluids.

1. Introduction

Forced convection analysis in the geometry of a channel is totally important issue in many technological applications like cooling of electronic components, heat exchanger systems, high performance boilers, chemical catalytic reactors, solar collectors, cooling of gas turbine blades and so on [1–10]. Management of heat transfer for its enhancement in these systems by improvements in cooling methods is an obligate task from an energy saving perspective. Increasing heat transfer performance is very important in macro- and micro-scales of channels [11]. Using extended surfaces in a channel is a practical method for increasing heat transfer coefficient. Comprehensive reviews of the relevant literature on this subject are given Incropera [12], Peterson and Ortega [13] and few more [14–16].

Detailed investigation of the effect of controlling parameters on the cooling of heated channels with mounted objects was performed by Young and Vafai [17] using the finite element method. Various parametric changes in the basic obstacle geometry, Reynolds number, solid thermal conductivity and heat input have been considered to see their effect on the flow and heat transfer. Motivated by vast applications in electronic system, Chung and Tucker [18] simulated the forced convection heat transfer in grooved channels. The heat transfer phenomena in a rectangular channel with angled ribs were numerically investigated by Lu and Jiang [19]. Their results indicated that the SST k-ω model was found to perform better than RNG k-ε when compared with experimental data. In addition, they also found that the channel with 20 ribs and 1 mm or 2 mm apart had the best thermal/hydraulic performance.

On other side of numerical history, the lattice Boltzmann method (LBM), a method based on the kinetic theory, has evolved as a robust and powerful numerical method for a wide range of complicated fluid flow problems [20–26] viscous, single and multiphase fluid flows [27–30] in science and engineering that are

* Corresponding authors at: Faculty of Mechanical Engineering, Universiti Teknologi Malaysia, 81310 UTM Skudai, Johor, Malaysia (N.A.C. Sidik).

E-mail addresses: rasul_mohebbi@du.ac.ir (R. Mohebbi), Izadi.m@lu.ac.ir (M. Izadi), azwadi@mail.fkm.utm.my (N.A.C. Sidik).

https://doi.org/10.1016/j.ijheatmasstransfer.2017.10.063
0017-9310/

Nomenclature

AR	aspect ratio of the cavity, a/b (dimensionless)
A	l/H, ratio between the blocks' distance to the channel's height
B	h/H, the extended surfaces' height to height of channel ratio
c	lattice speed [$m\,s^{-1}$]
cp	specific heat capacity at constant pressure [J/kg K]
dp	nanoparticle diameter [m]
e	streaming speed for single-particle
f	density distribution function
f^{eq}	equilibrium density distribution function
g	energy distribution function
g^{eq}	equilibrium energy distribution function
H	channel height [m]
h	heat transfer coefficient [$W\,m^{-2}\,K^{-1}$]
k	thermal conductivity [W/(m K)]
kB	Boltzmann constant [J/K]
L	length of the channel [m]
Nu	local Nusselt number
Pr	Prandtl number, ν/α
Re	Reynolds number, $u_{in}2H/\nu$
t	time [s]
T	temperature [K]
T_{in}	inlet temperature [K]
T_b	bulk temperature [K]
U_{in}	u-component at the channel inlet [$m\,s^{-1}$]
u, v	velocity components [$m\,s^{-1}$]
u	velocity vector [$m\,s^{-1}$]
X	the upstream face of the blocks
x, y	Cartesian coordinates [m]
x_u	dimensionless upstream face of the cavity, x/L
w	weight function
W	dimensionless bubble width, $\bar{W}_r/A$

Greek symbols

α	thermal diffusivity [$m^{-2}\,s^{-1}$]
β	thermal expansion coefficient [K^{-1}]
μ	dynamic viscosity [$kg\,m^{-1}\,s^{-1}$]
δx	lattice spacing [m]
δy	lattice spacing]m]
δt	time step [s]
ν	kinematic viscosity [m^2/s]
ρ	density of fluid [$kg\,m^{-3}$]
τ_g	dimensionless single relaxation time for the heat transfer computation
τ_ν	dimensionless single relaxation time for the flow computation
φ	solid volume fraction

Subscripts

c	cold
f	fluid
H	hot
i	move direction of single-particle
in	inlet
nf	nanofluid
p	particle
out	outlet
w	wall
′	dimensional quantity

problematic for conventional methods. Alamyane and Mohamad [15] considered LBM to investigate the forced convection regime in a channel with extended surfaces. Their focus was to test the effect of Reynolds number (*Re*) and extended surfaces' height and spacing. The authors concluded that the closer the objects the better the heat transfer and as the height of the objects increase, the temperature in spacing increases. Pirouz et al. [31] solved the conjugate heat transfer in a rectangular channel. They reported that reducing the distance between obstacles makes the flow deviate and accelerate in the vicinity of faces and causes an increase in the rate of convective heat transfer from the obstacles. Biswas et al. [6] studied the two-dimensional numerical simulations using the LBM to understand the effect of cross-buoyancy on the mixed convective flow and heat transfer in a ribbed channel. They concluded that heat transfer follows two mechanisms. First, heat transfer occurs due to thermal boundary layer interruption at the leading edge of rib and, second, enhanced heat transfer occurs beyond a critical *Re* due to the vortex shedding and mixing mechanisms.

On the other hand, improving the thermal conductivity of conventional fluids such as water, mineral oil and ethylene glycol has been the focus of research by many investigators. One of the innovative ways is by suspension of solid nanoparticles (1–100 nm diameter) in a base fluid, known as nanofluid [32–35]. The nanofluid is stable [36–39] and compared with suspended particles of millimeter-or-micrometer dimensions, which have numerous drawbacks like sedimentation, erosion, fouling and increased pressure drop of the flow channel, the nanofluids show much better stability and with acceptable pressure drop [40,41]. Also, nanofluids are expected to transfer heat at a higher rate than ordinary fluids [42–46]. Izadi and Partners [47–51] have performed comprehensive researches related to forced and mixed convection of nanofluids. For example, a numerical code has been developed to consider laminar forced convection of a nanofluid consisting of Al_2O_3 and water numerically [47]. The results showed the dependency of the friction coefficient on the nanoparticle concentration has a meaningful relationship with the magnitude of heating energy to the momentum energy. Anwar Beg et al. [52] studied a computational fluid dynamics simulation of laminar convection of Al_2O_3–water bio-nanofluids in a circular tube with constant wall temperature conditions. Their simulations showed that heat transfer coefficient distinctly increases with increasing nanofluid particle concentration. Rashidi et al. [53] investigated the laminar forced convection flow and heat transfer of Cu-water nanofluid for a wavy channel for a single phase and three different two-phase models predictions and they compared their results with each other. Garoosi et al. [54] studied natural convection heat transfer of nanofluid in a two-dimensional square cavity containing several pairs of heater and coolers, numerically.

There are also many studies concerning nanofluid simulation in channels using LBM [55–57]. Yang and Lai [56] performed LBM investigations on nanofluid heat transfer in a microchannel. They concluded that heat transfer performance increases with increasing Reynolds number and nanofluid concentration. Sidik et al. [57] studied the thermal efficiency by using LBM. Their research considered fin and nanofluid for heat transfer enhancement. They concluded that the heat transfer efficiency strongly depends of the Reynolds number and the conduction coefficient of the fins.

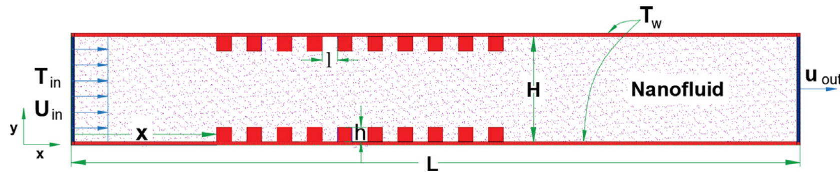

Fig. 1. Schematic illustration of the considered problem.

Table 1
Thermo-physical properties of the base fluid and the nanoparticles [51].

Property	Fluid phase (water)	CuO (nanoparticles)	Al_2O_3 (nanoparticles)	TiO_2 (nanoparticles)
C_p (J/kg K)	4179	383	765	686.2
ρ (kg/m^3)	997.1	8954	3970	4250
K (W/m K)	0.613	400	40	8.9538
$\beta \times 10^5$ (K_1)	21	1.67	0.85	0.9
$\mu \times 10^4$ (kg/ms)	8.55		–	

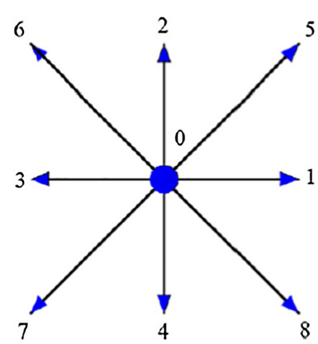

Fig. 2. D2Q9 lattice.

Based on our literature review, the study on forced heat transfer of nanofluids in a channel with rectangular blocks connects to its both upper and bottom walls for optimization of heat transfer performance is scarce. Therefore, the main goal of this work is to examine forced convection heat transfer in laminar regime using different type of nanofluids (CuO, Al_2O_3 and TiO_2) in a channel with extended using LBM. The main parameters controlling the fluid flow and heat transfer parameters inside the channel, such as Reynolds number, solid volume fraction, distance and heights of the blocks are investigated due to their importance for the heat transfer enhancement.

2. The study case

The forced convection heat transfer of the nanofluid in a two dimensional channel with blocks attached to up and bottom walls is numerically studied using lattice Botlzmann method. Details of configuration of considered work are shown in Fig. 1.

The channel aspect ratio is fixed at L/H = 25. Ten blocks are placed on inner side of top and bottom wall. The height and width of blocks are denoted with h and w, respectively. The ratio of distance between two consecutive blocks to the channel's height (A = l/H) is varied from 0.2 to 0.8. Also the extended surfaces' height to height of channel ratio (B = h/H) is varied from 0.05 to 0.35. The upstream blocks are located at distance x/L = 0.16 from the channel inlet. The Reynolds number varies from 10 to 70. The nanofluid enters to the channel with uniform velocity, u_0, and uniform temperature, T_0. The nanofluid as working fluid is cooler than the channel walls and blocks. The nanofluid and related flow are considered to be Newtonian, incompressible, and laminar. The nanofluids consist of solid spherical particles of 100 nm diameter. The buoyancy effects are negligible, as its effect is not so significant in comparison with the inertia force of flow. Table 1 shows the thermo-physical properties of the base fluid and the nano-particles.

3. Numerical simulation

3.1. Nanofluid thermophysical properties

Nanofluid has different behavior from pure liquid due to inter-particle potentials and other forces on the nanoparticles. Therefore, for numerical simulation of the nanofluid, some new equations should be considered for the properties. The thermophysical properties of the fluid are the functions of concentration and temperature. According to the classical formula for a solid–liquid mixture, the density of nanofluids ρ_{nf} can be estimated by [58–61]:

$$\rho_{nf} = (1-\phi)\rho_f + \phi\rho_p \tag{1}$$

where subscripts f, nf and p stand for base fluid, nanofluid and solid, respectively. Using the heat capacity of nanofluid [62], the nanofluid thermal diffusivity can be obtained by:

$$(\rho c_p)_{nf} = (1-\phi)(\rho c_p)_f + \phi(\rho c_p)_p \tag{2}$$

$$\alpha_{nf} = \frac{k_{nf}}{(\rho c_p)_{nf}} \tag{3}$$

The effective dynamic viscosity is expressed by using the Brinkman model [63]:

$$\mu_{nf} = \mu_f/(1-\phi)^{2.5} \tag{4}$$

The thermal conductivity of the nanofluid can be approximated by the Patel et al.'s model [64] which is

$$\frac{k_{nf}-k_f}{k_f} = \frac{k_p}{k_f}\left(1 + \mathrm{c}\frac{u_p d_p}{\alpha_f}\right)\frac{d_f}{d_p}\frac{\phi_p}{1-\phi_p} \tag{5}$$

where c is a constant and equal to 25,000 for a wide range of experimental data [64]. u_p is the Brownian velocity for nanoparticles and can be determined as:

$$u_p = \frac{2k_B\theta}{\pi\mu_l d_p^2} \tag{6}$$

In which k_B is the Boltzmann constant and θ is the temperature in Kelvin. The following equation can be used to compute the nanofluid Prandtl number:

$$\mathrm{Pr}_{nf} = \frac{(\mu c_p)_{nf}}{k_{nf}} \tag{7}$$

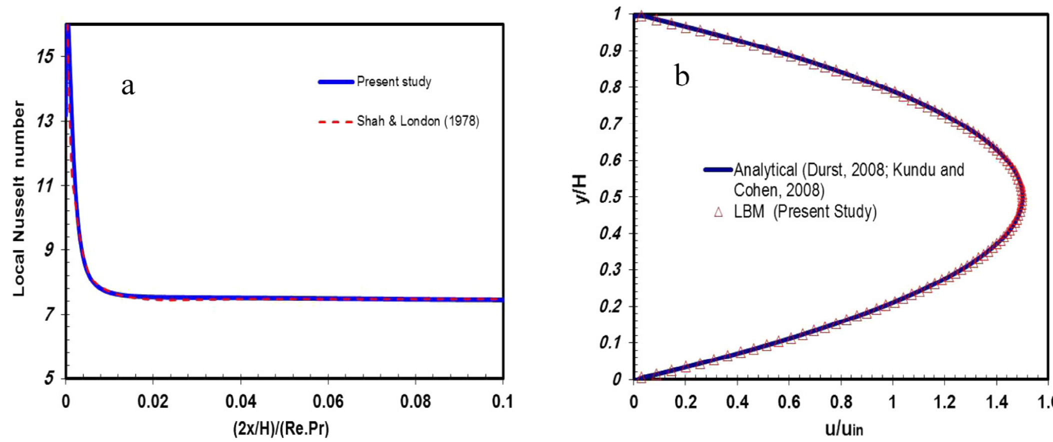

Fig. 3. (a) Comparison of local Nusselt number calculated at the lower wall of the plane channel with those obtained by Shah and London [83], (b) Comparison of present numerical results with the analytical exact solution.

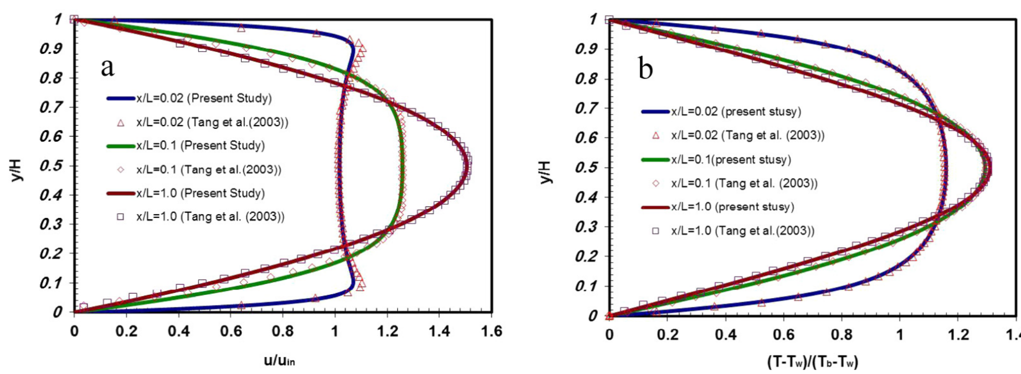

Fig. 4. Comparison of (a) velocity and (b) temperature profiles at different cross sections between the present study and Tang et al. [86].

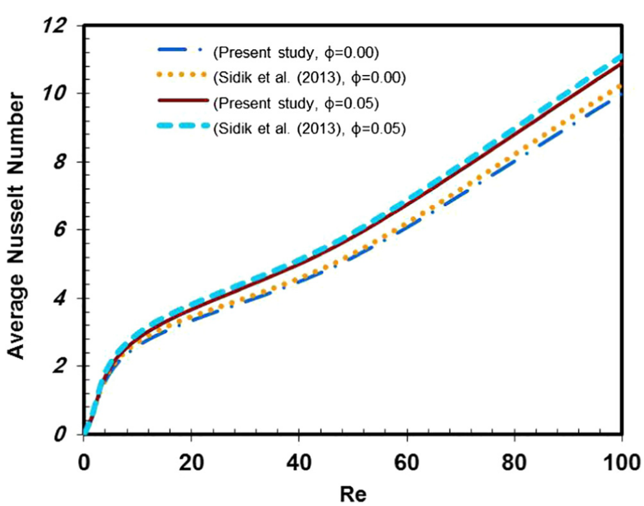

Fig. 5. Variation of average Nusselt number versus Reynolds number.

3.2. Lattice Boltzmann method

The starting point for lattice Boltzmann simulation is the evolution equation for a set of density distribution functions f_i which is discrete in both space and time [65]

$$f_i(\mathrm{x}+\mathrm{e}_i\delta t, t+\delta t) - f_i(\mathrm{x},t) = -\frac{1}{\tau_v}[f_i(\mathrm{x},t) - f_i^{eq}(\mathrm{x},t)] \tag{8}$$

where e is the particle's velocity, τ_v is the relaxation time for the collision, f_i^{eq} is an equilibrium distribution function and i = 0, 1,…8 for two-dimensional nine-velocity (D2Q9) model (Fig. 2). Noted that the right hand side of Eq. (8) is the collision term where the Bhatnagar–Gross–Krook (BGK) approximation has been applied [66].

The discrete velocity is expressed as [67]

$$\mathrm{e}_i = \begin{cases} (0,0) & (i=0) \\ (\cos[(i-1)\pi/2], \sin[(i-1)\pi/2])\cdot c & (i=1,\ldots,4) \\ \sqrt{2}(\cos[(i-5)\pi/2+\pi/4], \sin[(i-5)\pi/2+\pi/4])\cdot c & (i=5,\ldots,8) \end{cases} \tag{9}$$

where c = δx/δt, for the present case as uniform mesh has been chosen with δt = 1, δx = 1; hence c = 1 in the simulation. The equilibrium distribution function, f_i^{eq}, is chosen such that the continuum macroscopic equations approximated by evolution equation correctly describe the hydrodynamics of the fluid. For D2Q9 model, f_i^{eq} is defined as

$$f_i^{eq} = w_i\rho\left[1 + 3\frac{\mathrm{e}_i\cdot\mathrm{u}}{c^2} + \frac{9}{2}\frac{(\mathrm{e}_i\cdot\mathrm{u})^2}{c^4} - \frac{3}{2}\frac{\mathrm{u}^2}{c^2}\right] \tag{10}$$

where w_i has the values of $w_0 = 4/9$, $w_i = 1/9$ for i = 1 to 4 and w_i = 1/36 for i = 5 to 8. The relaxation time for the flow field, τ_v can be define as

$$\tau_v = 0.5 + \nu\frac{\delta t}{c_s^2} \tag{11}$$

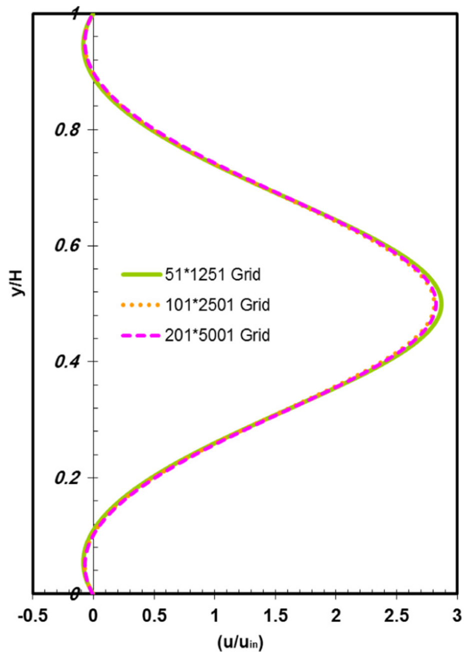

Fig. 6. Normalized velocity for different number of grids at x/L = 0.3, ϕ = 0.03, *Re* = 40, A = 1.0 and B = 0.3 for five blocks mounted in up and down wall.

Table 2
Effect of the mesh size on average Nusselt number for ϕ = 0.03, A = 1.0 and B = 0.3 for five blocks mounted in up and down wall.

Re	Number of nodes	Average Nusselt number	Percentage of error $\frac{\lvert Nu_{new}-Nu_{old}\rvert}{Nu_{new}}\times 100$
10	51 × 1251	10.1718	
	101 × 2501	9.9450	2.2805
	201 × 5001	9.9394	**0.0563**
40	51 × 1251	11.3467	
	101 × 2501	11.9077	4.7112
	201 × 5001	11.9034	**0.0361**
70	51 × 1251	12.1865	
	101 × 2501	12.2843	0.7961
	201 × 5001	12.2811	**0.0260**

The bold values represent the lattices number yielded the required accuracy of results and relevant relative variation of average Nusselt.

where ν is kinematic viscosity and $c_s = \frac{c}{\sqrt{3}}$ is the speed of sound. ν will be calculated by Reynolds number as

$$\nu = \frac{u_0 \cdot 2H}{Re} \tag{12}$$

In the LBM, the fluid macroscopic quantities such as ρ and flow momentum, ρu, are calculated by using the distribution function f_i, and given by

$$\rho = \sum_{i=0}^{8} f_i \tag{13}$$

$$\rho \mathrm{u} = \sum_{0}^{8} f_i \mathrm{e}_i \tag{14}$$

Prediction of thermal field requires a new type of distribution function to represent the evolution of internal energy [68–72]. A thermal distribution function g_i is used to solve the energy equation for evaluating the value of temperature field. A similar approach is also suggested by Mohamad [73]. The discretized the simplified doubled population thermal lattice BGK model proposed by Yan and Zu [74] is given as

$$g_i(x + \mathrm{e}_i\delta t, t + \delta t) - g_i(x, t) = -\frac{1}{\tau_g}[g_i(x, t) - g_i^{eq}(x, t)] \tag{15}$$

The above expression is similar to the discretized LBM equation used to solve momentum in Eq. (8). Here, τ_g is a single relaxation collision frequency for temperature distribution function and can be defined as

$$\tau_g = 3\alpha + 0.5 \tag{16}$$

where α can calculated by the value of a fixed parameter Pr = ν/α. The expression for g_i^{eq} is given as [75]

$$g_i^{eq} = w_i T\left[1 + 3\frac{\mathbf{e}_i \cdot \mathbf{u}}{c^2}\right] \tag{17}$$

where the value of the macroscopic fluid temperature can be evaluated from [76]

$$T = \sum_{i=0}^{8} g_i \ldots (i = 0, 1, \ldots, 8) \tag{18}$$

The Chapman-Enskog expansion can be used in the lattice Boltzmann method (LBM) to derive following macroscopic mass, momentum and energy equations. Details derivation can be found in Refs. [77,78].

The governing equations of continuity, momentum and energy are expressed as follow:

Continuity equation

$$\nabla \cdot (\rho_{nf}\mathbf{u}_{nf}) = 0 \tag{19}$$

Momentum equation

$$\nabla \cdot (\rho_{nf}\mathbf{u}_{nf}\mathbf{u}_{nf}) = -\nabla P + \nabla \cdot (\mu_{nf}\nabla\mathbf{u}_{nf}) + \rho_{nf}\mathbf{g} \tag{20}$$

Energy equation

$$\nabla \cdot (\rho_{nf}C_{p,nf}T_{nf}\mathbf{u}_{nf}) = \nabla \cdot (k_{nf}\nabla T_{nf}) \tag{21}$$

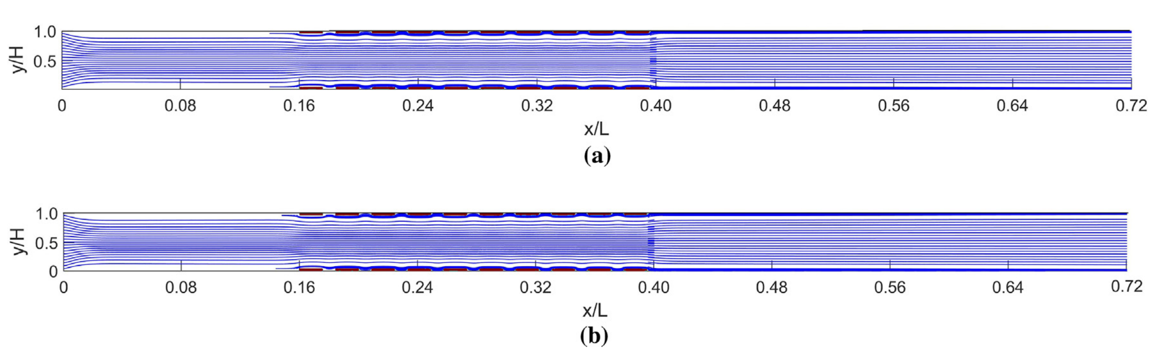

Fig. 7. Variations of the streamlines in the channel versus ϕ at R = 10, A = 0.2 and B = 0.05, (a) ϕ = 0.0, (b) 0.05.

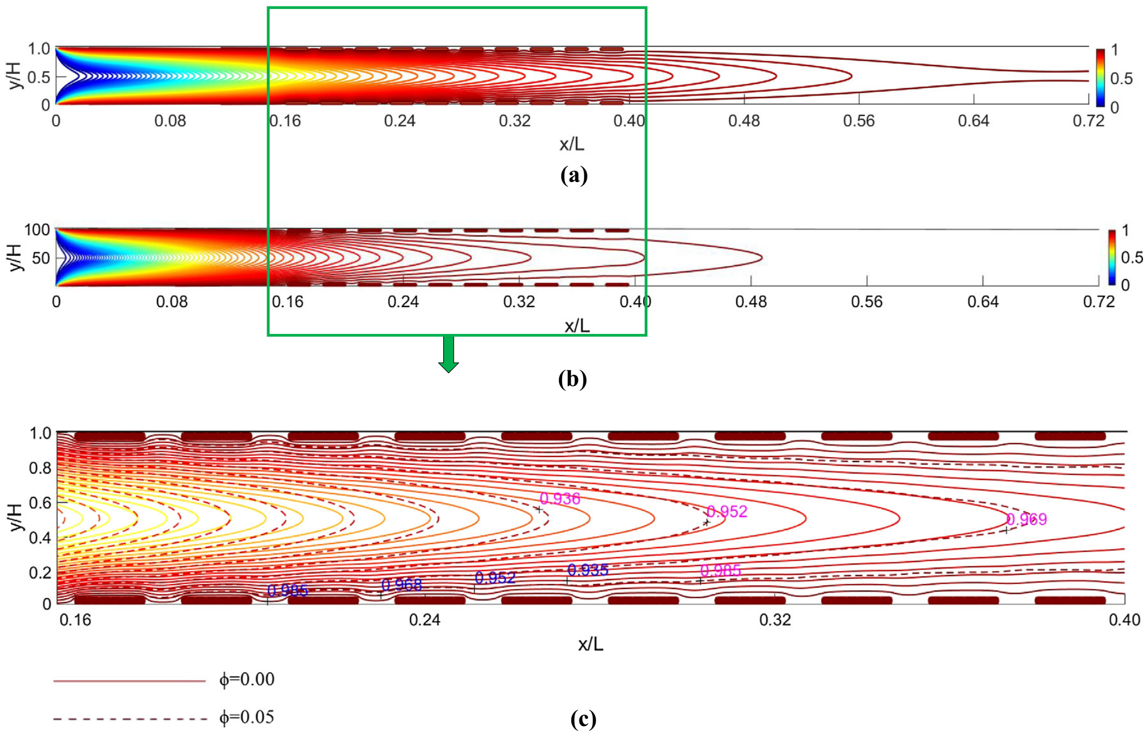

Fig. 8. Variations of the isotherms in the channel at *Re* = 10 for A = 0.2 and B = 0.05, (a) ϕ = 0.0, (b) 0.05, (c) comparisons of dimensionless isotherm contours for the pure fluid (ϕ = 0.0) and nanofluid (ϕ = 0.05).

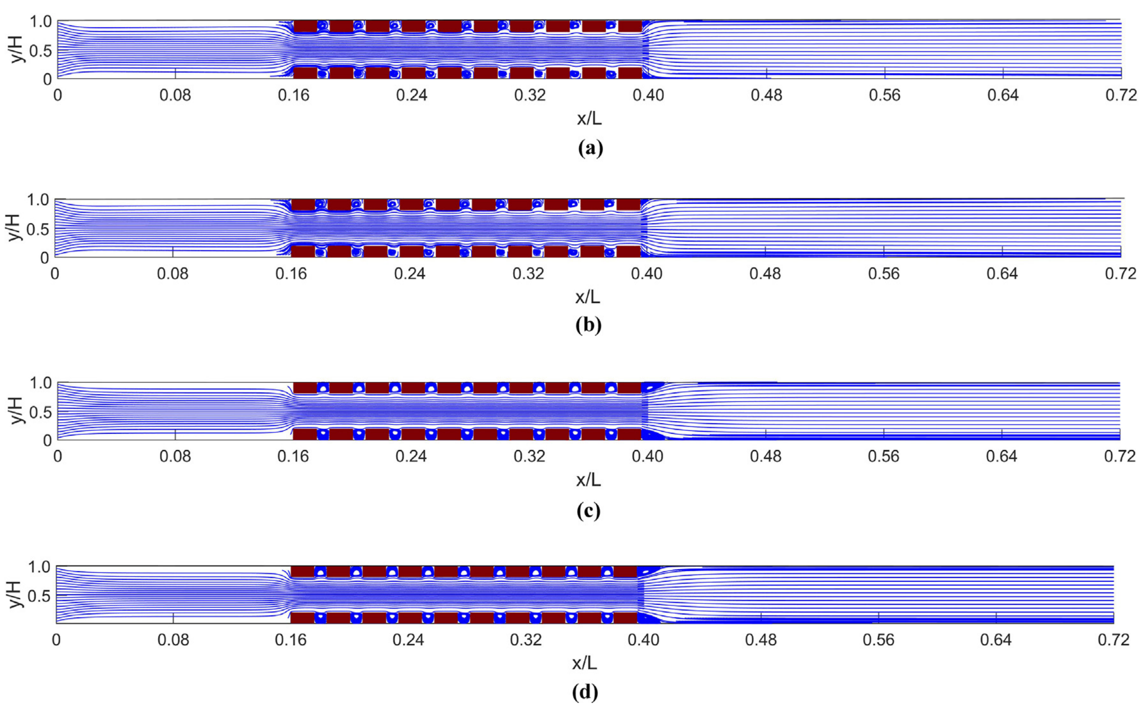

Fig. 9. Variations of the streamlines throughout the channel for A = 0.2 and B = 0.20, (a) *Re* = 10, ϕ = 0 (b) *Re* = 10, ϕ = 0.05 (c) *Re* = 70, ϕ = 0 and (d) *Re* = 70, ϕ = 0.05.

4. Numerical strategy and boundary conditions

Generally, two important steps in lattice Boltzmann method are i.e. streaming and collision. From the streaming process, the distribution functions out of the domain are known. Regarding the boundary conditions of the flow field, the solid walls are assumed to be no slip, and thus the bounce-back scheme is applied [79–81]. The Zou–He model [80] was used at the inlet of the computational domain in the LBM. An extrapolation scheme, as proposed by Mei et al. [82], is used to simulate the outlet flow condition in LBM. The constant temperature was considered for thermal boundary condition of two inner walls and mounted blocks. The inlet flow velocity and temperature of nanofluid set to be uniform. Here, the method introduced by Mohamad [75] was employed to treat the constant

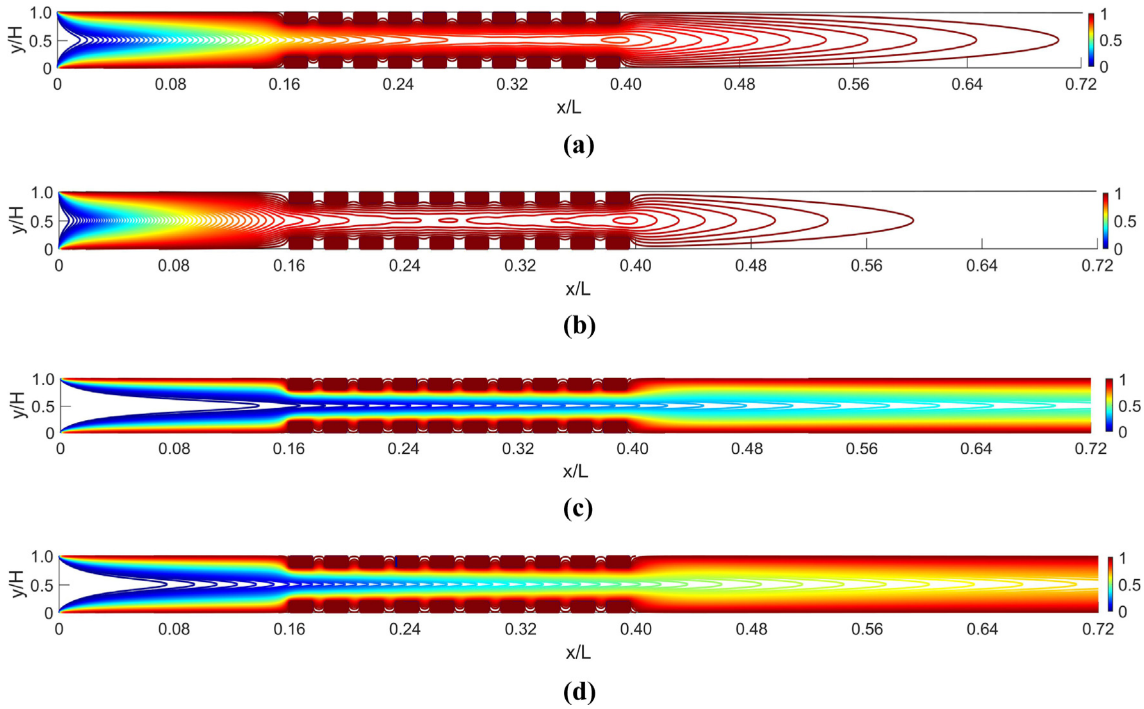

Fig. 10. Variations of the isotherms throughout the channel for A = 0.2 and B = 0.20 (a) Re = 10, ϕ = 0 (b) Re = 10, ϕ = 0.05 (c) Re = 70, ϕ = 0 and (d) Re = 70, ϕ = 0.05.

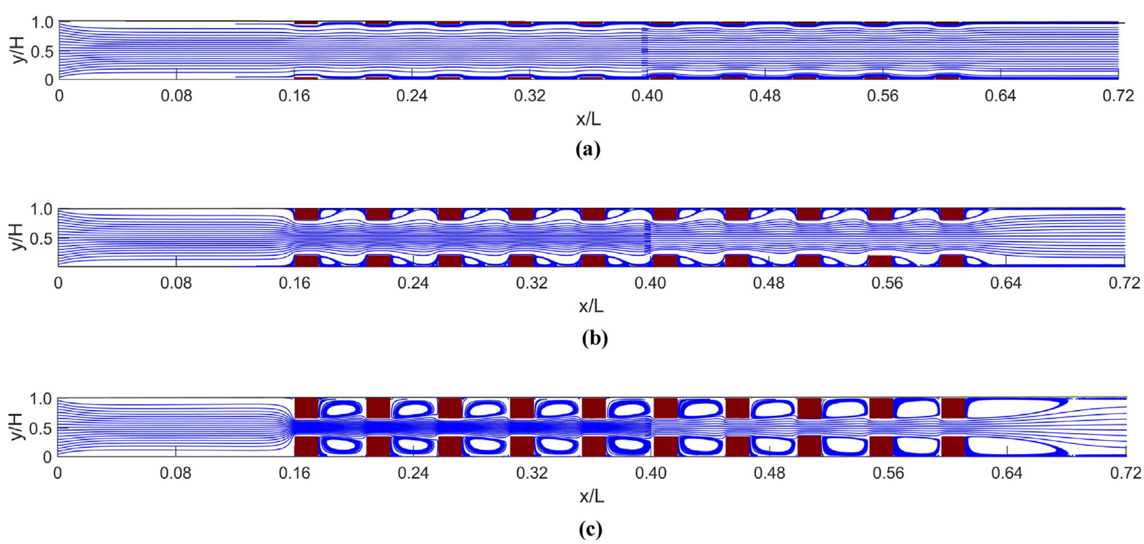

Fig. 11. Variations of the streamlines in the channel versus B for Re = 70, A = 0.8 and ϕ = 0.05, (a) B = 0.05, (b) B = 0.20, (c) B = 0.35.

temperature boundary conditions. In the present study also, the viscous dissipation, radiation, gravitational force, and Brownian effects were not considered.

5. Code validation and accuracy of the numerical simulation

A homemade FORTRAN program was developed for numerical simulation. During each simulation, the memory space usage was 101 MB and the CPU usage was 13% of Intel(R) core(TM) i7 CPU Q720@1.60 GHz. To check the convergence of the sequential iterative solution, the relative differences of u, v, and T at each node between two successive iterations are less than a prescribed value of 10^{-6}. The numerical method in the present research completely validated. The first verification is for a channel with parallel plates, all the walls are heated with a constant temperature and the water is used as fluid working. The local Nusselt number is defined as:

$$Nu = -\frac{2H.\frac{\partial T}{\partial y}|_{y=0}}{T_w - T_b} \tag{22}$$

where Tb given by,

$$T_b = \frac{\int_0^H u \cdot T dy}{\int_0^H u \, dy} \tag{23}$$

The local Nusselt number at the lower wall of the channel versus non-dimensional longitudinal coordinate (2×/H)/($Re \cdot Pr$) is shown in Fig. 3a. It is seen that the results of the present study

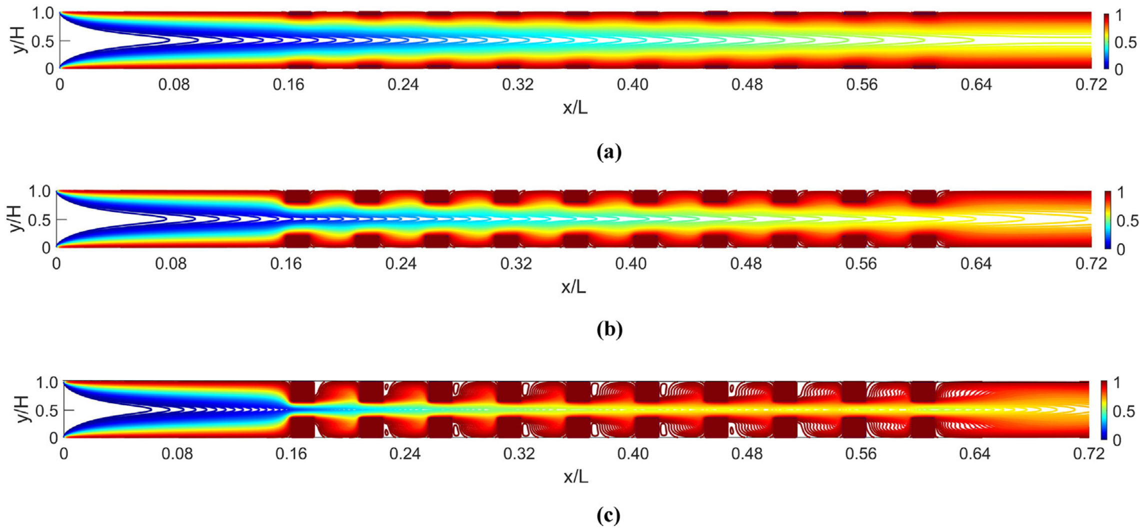

Fig. 12. Variations of the isotherms in the channel versus B for Re = 70, A = 0.8 and ϕ = 0.05, (a) B = 0.05, (b) B = 0.20, (c) B = 0.35.

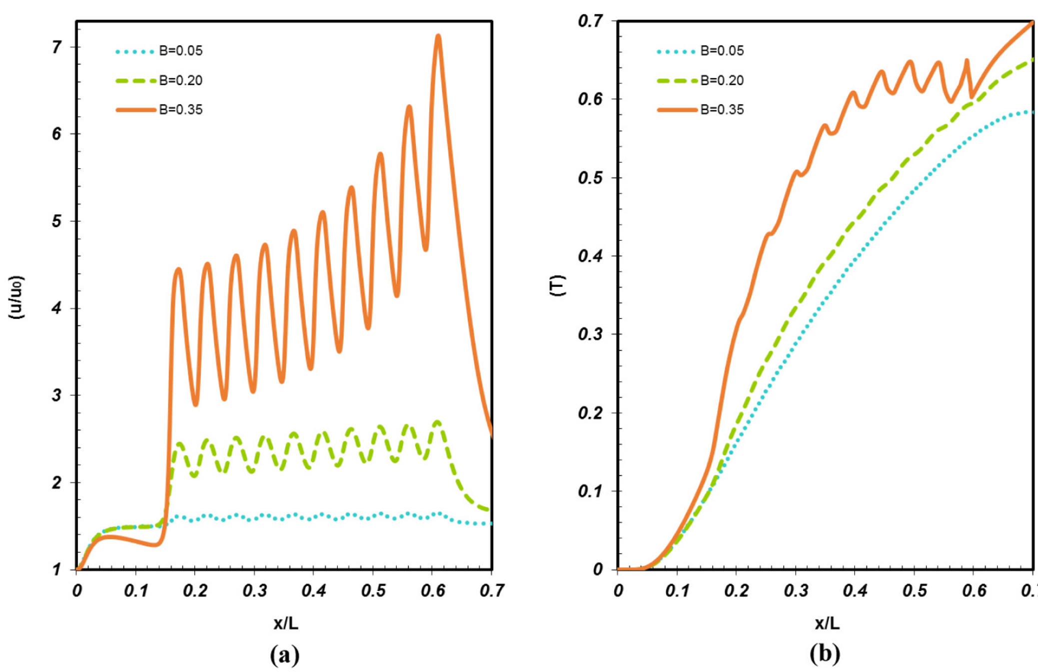

Fig. 13. (a) Normalized velocity profiles, (b) dimensionless temperature profile along the centerline of channel at Re = 70, A = 0.8 and ϕ = 0.05.

are in good agreement with previous data [83]. In addition, Fig. 3b is presented a comparison between the numerical solution and the analytical one.

The analytical solution for the incompressible fully developed flow between two parallel plates can be define as [84,85]:

$$\frac{u}{u_{in}} = \frac{3}{2}\left(\frac{4y}{H} - \left(\frac{2y}{H}\right)^2\right) \tag{24}$$

The comparison shows, the LBM results are highly accurate and are in good agreement with theoretical parabola.

The second comparison is concerned with comparison between the present model and the numerical results of Tang et al. [86] for a channel with uniform inlet velocity at Re = 10. The profiles of the normalized velocity, u/u_{in} and the normalized temperature, $(T - T_w)/(T_b - T_w)$, at three cross sections are shown in Fig. 4a and b. The comparisons show a good concurrence between the results.

Finally, the third test of the code validity was chosen for thermal efficiency of fins collocated on the bottom wall of a horizontal channel. The lower wall of the channel is at constant temperature and cooled by mixed convection in laminar flow regime [57]. In this case, the average Nusselt number for various Reynolds number, ϕ = 0 and 0.05 are applied. As shown in Fig. 5, a very good agreement is observed for different values of the Reynolds number and nanoparticles volume fraction. To demonstrate the independent of results from the grid size and finally choosing a suitable grid for the computational domain, the solution has been done for three difference meshes as 51 × 1251, 101 × 2501 and 201 × 5001 in y and x-directions, respectively. There is no noticeable

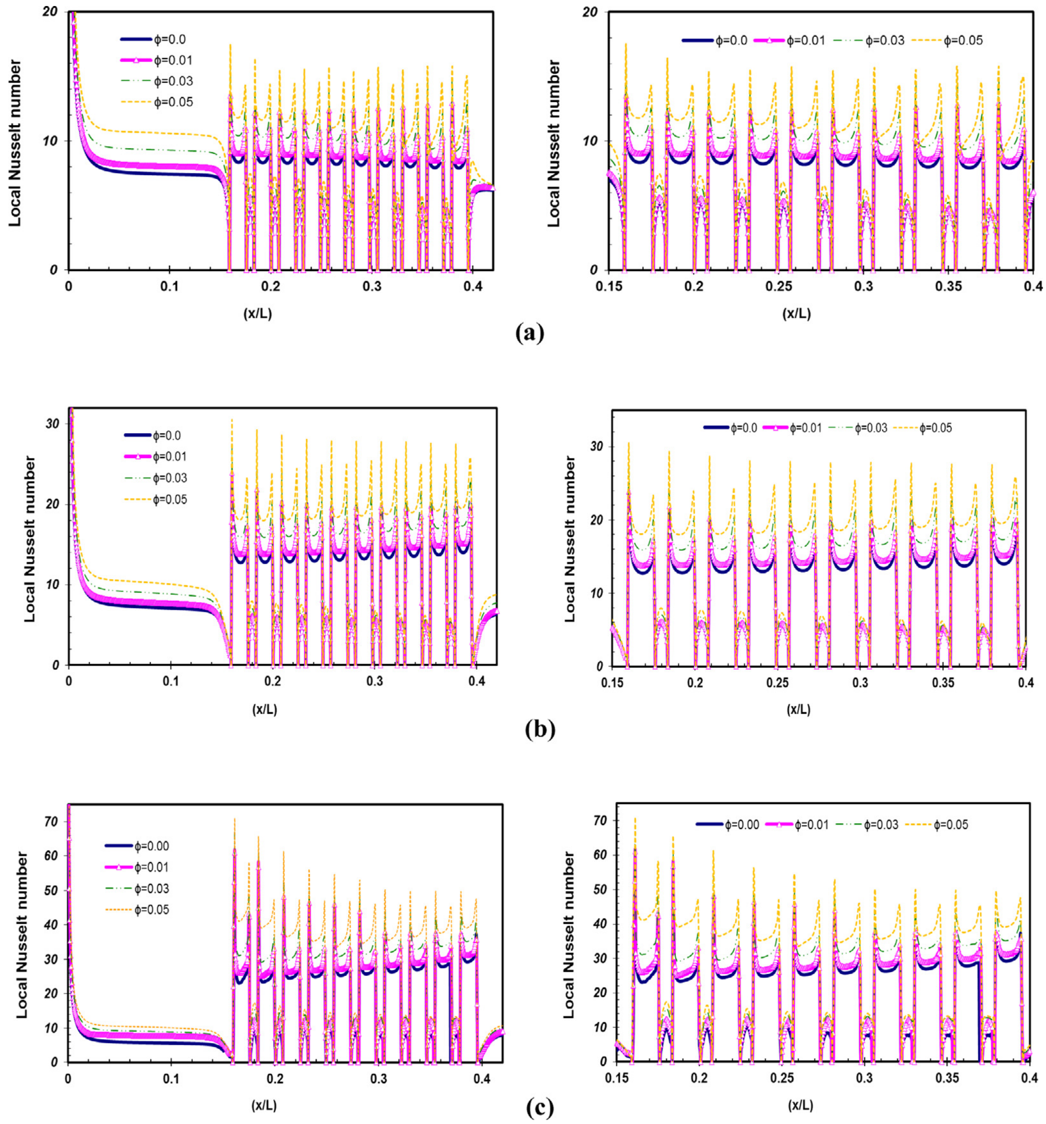

Fig. 14. Local Nusselt number in different volume fraction of nanofluid for *Re* = 10, A = 0.2, (a) B = 0.05, (b) B = 0.20, (c) B = 0.35.

difference between the results as presented in Fig. 6. In addition, the effect of the grid size on the average Nusselt number, calculated for bottom wall, at different Reynolds number is given in Table 2. The results showed difference is less than 1% between the studied grid size of 101 × 2501 and 201 × 5001. Combination of 101 × 2501 lattices number yielded the required accuracy and therefore it was chosen as the final independent lattice numbers in this work by considering the computational cost and numerical accuracy.

6. Results and discussion

This study presents the flow and temperature fields for different values of the Reynolds number, i.e. *Re* = 10, 40 and 70, wide range of solid volume fraction. i.e. φ = 0.00, 0.01, 0.03 and 0.05, different the geometric parameter, i.e. A = 0.2, 0.5 and 0.8 and also different relative height of the extended surfaces, i.e. B = 0.05, 0.20 and 0.35.

6.1. Case of A = 0.2

6.1.1. Blocks with relative height B = 0.05

Figs. 7 and 8 show the streamlines and isotherms contours for different volume fraction of solid phase at R = 10, A = 0.2 and B = 0.05. For comparison in isotherms, both the results of base fluid (solid lines) and the nanofluid (ϕ = 0.05) are presented by enlarging in Fig. 8c.

According to Fig. 7, the nanofluid flow affected by the extended surfaces in up and down wall of channel. In this case, there is not any circulation zone behind the block. Because the height of extended surfaces is lesser than blocks' distance, so the low pressure zones are very small in channel. In addition, presence of extended surfaces slightly disturbs the isotherms (see Fig. 8). It is found that, the thermal boundary layer thickness is bigger for ϕ = 0.05 (see Fig. 8c). This phenomenon was explained by Heidary and Kermani [87]. In addition, the length of developing region is shorter for nanofluid contrasted with pure fluid because of higher thermal diffusion through nanofluid.

6.1.2. Blocks with relative height B = 0.20

The effect of nanoparticle volume fraction and Reynolds number on the streamlines and isotherms of channel flow for A = 0.2 and B = 0.20 are shown in Figs. 9 and 10. Fig. 9 shows the formation of the vortexes behind the extended surfaces by increasing B, which are not created at B = 0.05 (see Fig. 7). Formation of the vortexes arises from low-pressure region between two successive

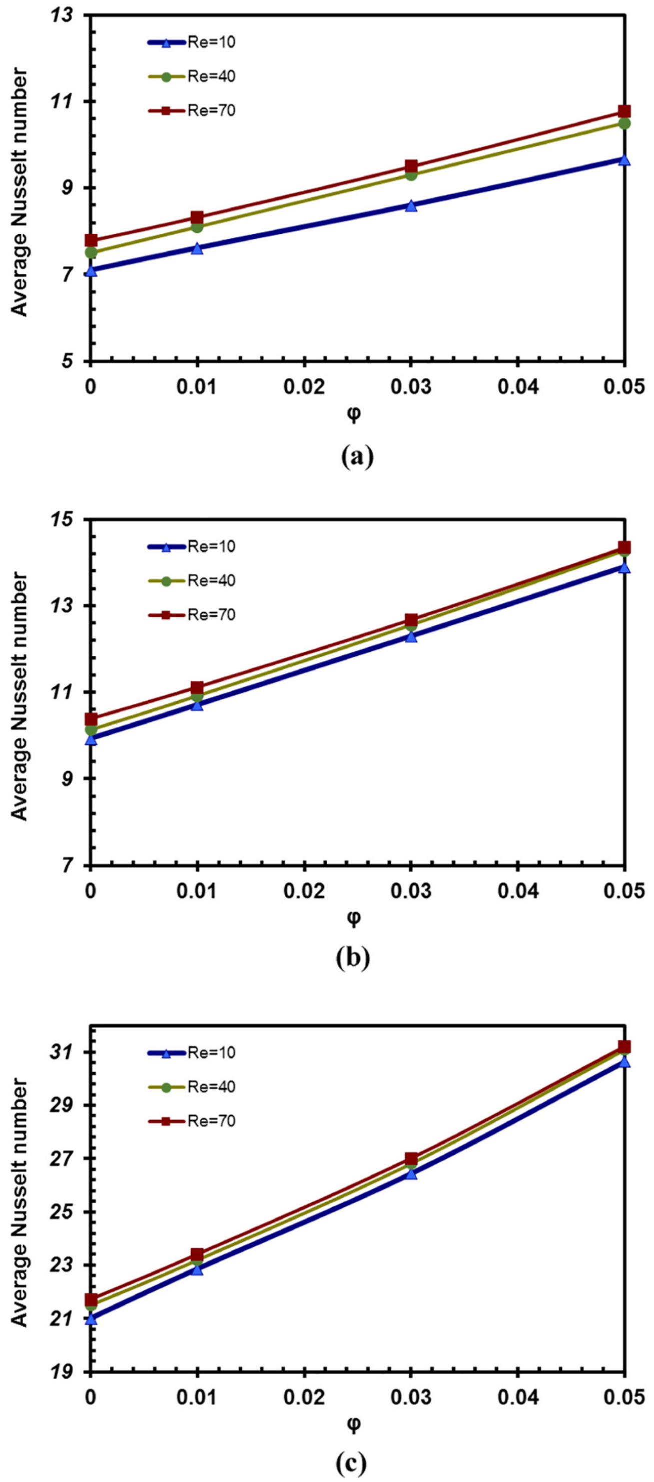

Fig. 15. The averaged Nusselt number for different solid volume fraction of nanofluid and various Reynolds numbers for A = 0.2, (a) B = 0.05, (b) B = 0.20, (c) B = 0.35.

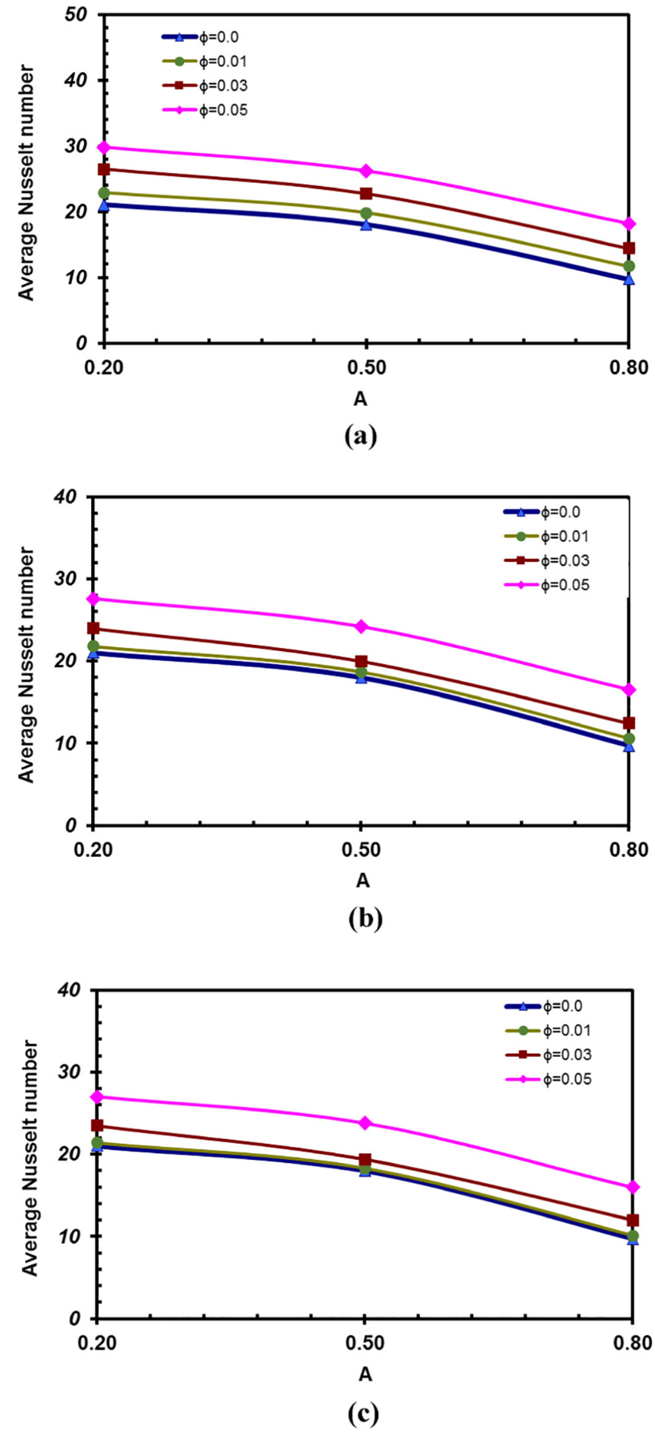

Fig. 16. The averaged Nusselt number for different solid volume fraction of nanofluid, different nanofluids and various blocks' distance for B = 0.35 and *Re* = 10, (a) CuO, (b) Al_2O_3, (c) TiO_2.

attached blocks. Higher value of Reynolds number leads to formation of bigger and stronger vorticities which occupying the whole space between the blocks. These vortexes connected with hot surface of blocks could contribute at the cooling of channel wall.

There is not any meaningful effect on the streamlines by changing the solid volume fractions of nanofluid. The effect of increasing in Reynolds number on the isotherms is presented in Fig. 10. As

Table 3
Effect of different nanofluids on percentage increase of the average Nusselt number to corresponding the pure water at different A for $\phi = 0.05$ and Re = 10.

A	CuO	Al_2O_3	TiO_2
0.2	41.90%	33.42%	29.57%
0.5	45.55%	35.42%	32.73%
0.8	87.62%	70.10%	64.94

clearly observed, thermal developing length increases and approach close to blocks by growth of *Re*. Also, the gradient of temperature in upper and lower wall of channel has more significant by increasing *Re*. For higher value of *Re*, isotherms completely develop through the region between the blocks. It is clear from this figure the temperature of nanofluid is higher than the pure water in every axial point of the channel, this is due to the higher thermal conductivity of the nanofluid which intensify the thermal diffusivity. Similar tests were performed in the case of B = 0.35, but the results are not presented here for reason of brevity.

6.2. Case of A = 0.8

The effect of changing the height of extended surfaces on streamlines and isotherms are also investigated at fixed A = 0.8, ϕ = 0.05 and *Re* = 70. The results are shown in Figs. 11 and 12. It is clear from the figure that for B = 0.05 there is not any vortex in channel. At higher B (Fig. 11b and c), larger recirculating eddies are formed and cover more area behind the obstacles. The biggest is created in the last obstacles for B = 0.35. This vortex located behind of last block could cause noticeable pressure loss inside of channel.

Uniformity of the temperature distribution through the channel diminishes by increment of B because of the more resistance in fluid flow subjected to greater extended surfaces. It is shown that by increasing B, the bigger vortices make a hotter zone in downstream of obstacle series.

Fig. 13 delineates the variations of normalized velocity and dimensionless temperature profile along the centerline of channel for *Re* = 70, A = 0.8 and ϕ = 0.05. According to this figure, the larger B produces the highest velocity and temperature, which leads to increase the heat transfer coefficient at bigger height of extended surfaces.

Enhancement of axial velocity could remove further amount of thermal energy and improve thermal efficiency of channel flow. It should be mentioned that the similar profile for other cases are not shown here for brevity.

The variation of local Nusselt number along the channel for different solid volume fractions of nanofluid and various height of obstacles is shown in Fig. 14 at *Re* = 10. According to the figure, the local Nu number decreases along the channel, but in the region near the blocks increases because of the high temperature gradient and immediately decrease in the space between the obstacles where vortices are formed. In all cases, it is obvious that the Nu number increases by increasing the ϕ and as a result of increased thermal conductivity of nanofluid.

Fig. 15 shows the effects of the nanoparticle volume fraction on the average Nusselt number of the channel flow at different *Re*. The outcomes show that the average *Nu* number increases by ϕ at a given *Re* and B, which it represents the average Nusselt number of nanofluid is higher than that of pure fluid. In addition, at a fixed ϕ and B, the average Nusselt number increases with increment of *Re*. Also, It is distinct that the average Nusselt number has a direct relationship with B.

The effect of changing in the space between obstacles (A) is also investigated and shown in Fig. 16a. By increasing the distance between the obstacles and hence expanding the recirculation formed behind each obstacle (see Figs. 9d and 11b), the average Nusselt number decreases. These vortices prevent from formation of direct connection between main axial flow and hot wall so that reduces *Nu* number.

Fig. 16a–c compares various nanofluids consisting of CuO, Al_2O_3 and TiO_2 nanoparticles, respectively. It can be seen that behavior of various nanofluid has similar trends, which the CuO-nanofluid contains the maximum effect on increasing the heat transfer. The minimum effect belongs to nanofluid with TiO_2 nanoparticles. In Table 3, Effect of using different nanofluids on increasing the average Nusselt number compared with pure water at different A are presented. By utilizing the nanofluid instead of the pure water, the heat transfer increases. Also, nanofluid contained CuO nanoparticles has better performance compared the other ones.

7. Conclusion

A LBM has been carried out in this study to investigate the forced convection flow of the nanofluids in a channel with extended surfaces attached to its both walls on the effect of changing different parameters such as solid volume fraction, *Re*, obstacles' height, and spacing between them. The highlights of the present study are summarized as follows:

- Higher value of Reynolds number leads to formation of bigger and stronger vortexes which occupying the whole space between the blocks. These vortexes connected with hot surface of blocks could contribute at the cooling of channel wall.
- Thermal developing length increases and approach close to blocks by increasing *Re*.
- Temperature of nanofluid is higher than the pure water in every axial point of the channel flow.
- The rate of heat transfer is decrease by increasing the spacing between the extended surfaces.
- Enhancement of axial velocity arised from increasing in B could remove further amount of thermal energy and improve thermal efficiency of channel flow.
- The predicted average Nusselt number increases with increase in height of the obstacles
- Comparison with other nanofluids indicates that CuO-nanofluid contrasted to other type performs a better enhancement heat transfer.

Conflict of interest

There is no conflict of interest to declare.

References

[1] M. Nazari, M. Kayhani, R. Mohebbi, Heat transfer enhancement in a channel partially filled with a porous block: lattice Boltzmann method, Int. J. Mod. Phys. C 24 (09) (2013) 1350060.

[2] M. Nazari, R. Mohebbi, M. Kayhani, Power-law fluid flow and heat transfer in a channel with a built-in porous square cylinder: lattice Boltzmann simulation, J. Non-Newtonian Fluid Mech. 204 (2014) 38–49.

[3] R. Mohebbi, M. Nazari, M. Kayhani, Comparative study of forced convection of a power-law fluid in a channel with a built-in square cylinder, J. Appl. Mech. Tech. Phys. 57 (1) (2016) 55–68.

[4] M. Jamil et al., Numerical study of separation length of flow through rectangular channel with baffle plates, J. Adv. Res. Des. 7 (1) (2015) 19–33.

[5] A. Razali, A. Sadikin, CFD simulation study on pressure drop and velocity across single flow microchannel heat sink, J. Adv. Res. Des. 8 (2015) 12–21.

[6] S. Biswas et al., Analysis of mixed convective heat transfer in a ribbed channel using the lattice Boltzmann method, Numer. Heat Transfer, Part A: Appl. 68 (1) (2015) 75–98.

[7] G. Ny et al., Numerical study on turbulent-forced convective heat transfer of Ag/Heg water nanofluid in pipe, J. Adv. Res. Mater. Sci. 22 (1) (2016) 11–27.

[8] R. Mohebbi, H. Heidari, Lattice Boltzmann simulation of fluid flow and heat transfer in a parallel-plate channel with transverse rectangular cavities, Int. J. Mod. Phys. C 28 (2017) 1750042.

[9] R. Mohebbi, M. Rashidi, Numerical simulation of natural convection heat transfer of a nanofluid in an L-shaped enclosure with a heating obstacle, J. Taiwan Inst. Chem. Eng. 72 (2017) 70–84.

[10] R. Mohebbi, H. Lakzayi, Nor Azwadi Che Sidik., Japar. Wan Mohd Arif Aziz, Lattice Boltzmann Method Based Study of the Heat Transfer Augmentation Associated with Cu/Water Nanofluid in a Channel with Surface Mounted Blocks, Int. J. Heat Mass Transf 117 (2018) 425–435.

[11] S. Abubakar, C.N. Azwadi, A. Ahmad, The use of Fe3O4-H2O4 nanofluid for heat transfer enhancement in rectangular microchannel heatsink, J. Adv. Res. Mater. Sci. 23 (2016) 15–24.

[12] F. Incropera, Convection heat transfer in electronic equipment cooling, ASME, Trans., J. Heat Transfer 110 (1988) 1097–1111.

[13] G. Peterson, A. Ortega, Thermal control of electronic equipment and devices, Adv. Heat Transfer 20 (1990) 181–314.
[14] T. Mugilan, N.A.C. Sidik, W.M.A.A. Japar, Akademia Baru, J. Adv. Res. Mater. Sci. 32 (1) (2017) 1–12.
[15] A.A. Alamyane, A. Mohamad, Simulation of forced convection in a channel with extended surfaces by the lattice Boltzmann method, Comput. Math. Appl. 59 (7) (2010) 2421–2430.
[16] V. Yadav et al., Numerical investigation of heat transfer in extended surface microchannels, Int. J. Heat Mass Transfer 93 (2016) 612–622.
[17] T.J. Young, K. Vafai, Convective cooling of a heated obstacle in a channel, Int. J. Heat Mass Transfer 41 (20) (1998) 3131–3148.
[18] Y.M. Chung, P.G. Tucker, Numerical studies of heat transfer enhancements in laminar separated flows, Int. J. Heat Fluid Flow 25 (1) (2004) 22–31.
[19] B. Lu, P.-X. Jiang, Experimental and numerical investigation of convection heat transfer in a rectangular channel with angled ribs, Exp. Therm. Fluid Sci. 30 (6) (2006) 513–521.
[20] N.A.C. Sidik, S.A. Razali, Various speed ratios of two-sided lid-driven cavity flow using lattice Boltzmann method, J. Adv. Res. Fluid Mech. Therm. Sci. 1 (2014) 11–18.
[21] A. Ismail, L. Jahanshaloo, A. Fazeli, Lagrangian grid LBM to predict solid particles' dynamics immersed in fluid in a cavity, J. Adv. Res. Fluid Mech. Therm. Sci. 3 (1) (2014) 17–26.
[22] H. Wang, Z. Qu, L. Zhou, A combined GCMC and LBM simulation method for CH 4 capture in Cu-BTC particle adsorption bed, Int. Commun. Heat Mass Transfer 88 (2017) 48–53.
[23] Z.-X. Tong et al., Analysis and numerical tests of lifting relations to reconstruct LBM distribution functions for coupling simulations, Int. J. Heat Mass Transfer 107 (2017) 945–955.
[24] M. Basha, N.A.C. Sidik, Numerical predictions of laminar and turbulent forced convection: Lattice Boltzmann simulations using parallel libraries, Int. J. Heat Mass Transfer 116 (2018) 715–724.
[25] M. Basha, N.A.C. Sidik, Numerical simulation of fluid flow and heat transfer in rotating channels using parallel lattice Boltzmann method, Int. J. Heat Mass Transfer 115 (2017) 158–168.
[26] G. Kefayati, Heat transfer and entropy generation of natural convection on non-Newtonian nanofluids in a porous cavity, Powder Technol. 299 (2016) 127–149.
[27] T. Inamuro, Lattice Boltzmann methods for viscous fluid flows and for two-phase fluid flows, Fluid Dyn. Res. 38 (9) (2006) 641–659.
[28] Y. Yan, Y. Zu, B. Dong, LBM, a useful tool for mesoscale modelling of single-phase and multiphase flow, Appl. Therm. Eng. 31 (5) (2011) 649–655.
[29] M. Basha, C.N. Azwadi, Numerical study on the effect of inclination angles on natural convection in entrance region using regularised lattice Boltzmann BGK, J. Adv. Res. Fluid Mech. Therm. Sci. 10 (1) (2015) 11–26.
[30] G.R. Kefayati, FDLBM simulation of magnetic field effect on mixed convection in a two sided lid-driven cavity filled with non-Newtonian nanofluid, Powder Technol. 280 (2015) 135–153.
[31] M.M. Pirouz et al., Lattice Boltzmann simulation of conjugate heat transfer in a rectangular channel with wall-mounted obstacles, Sci. Iranica 18 (2) (2011) 213–221.
[32] Y. Xuan, Q. Li, Heat transfer enhancement of nanofluids, Int. J. Heat Fluid Flow 21 (1) (2000) 58–64.
[33] N.C. Sidik, O.A. Alawi, Computational investigations on heat transfer enhancement using nanorefrigerants, J. Adv. Res. Des. 1 (1) (2014) 35–41.
[34] M.R. Abdulwahab, A numerical investigation of turbulent magnetic nanofluid flow inside square straight channel, J. Adv. Res. Fluid Mech. Therm. Sci. 1 (1) (2014) 44–52.
[35] G. Kefayati, Mixed convection of non-Newtonian nanofluid in an enclosure using Buongiorno's mathematical model, Int. J. Heat Mass Transfer 108 (2017) 1481–1500.
[36] D. Zhou, Heat transfer enhancement of copper nanofluid with acoustic cavitation, Int. J. Heat Mass Transfer 47 (14) (2004) 3109–3117.
[37] N. Noh, A. Fazeli, N.C. Sidik, Numerical simulation of nanofluids for cooling efficiency in microchannel heat sink, J. Adv. Res. Fluid Mech. Therm. Sci. 4 (1) (2014) 13–23.
[38] D. Jehad, G. Hashim, Numerical prediction of forced convective heat transfer and friction factor of turbulent nanofluid flow through straight channels, J. Adv. Res. Fluid Mech. Therm. Sci. 8 (1) (2015) 1–10.
[39] G. Kefayati, N.A.C. Sidik, Simulation of natural convection and entropy generation of non-Newtonian nanofluid in an inclined cavity using Buongiorno's mathematical model (Part II, entropy generation), Powder Technol. 305 (2017) 679–703.
[40] M.H. Hamzah et al., Factors affecting the performance of hybrid nanofluids: a comprehensive review, Int. J. Heat Mass Transfer 115 (2017) 630–646.
[41] G.R. Kefayati, FDLBM simulation of mixed convection in a lid-driven cavity filled with non-Newtonian nanofluid in the presence of magnetic field, Int. J. Therm. Sci. 95 (2015) 29–46.
[42] M. Rashidi et al., Lie group solution for free convective flow of a nanofluid past a chemically reacting horizontal plate in a porous media, Math. Problems Eng. 2014 (2014).
[43] N. Freidoonimehr, M.M. Rashidi, S. Mahmud, Unsteady MHD free convective flow past a permeable stretching vertical surface in a nano-fluid, Int. J. Therm. Sci. 87 (2015) 136–145.
[44] M.H. Abolbashari et al., Analytical modeling of entropy generation for Casson nano-fluid flow induced by a stretching surface, Adv. Powder Technol. 26 (2) (2015) 542–552.
[45] A. Afifah, S. Syahrullail, N.C. Sidik, Natural convection of alumina-distilled water nanofluid in cylindrical enclosure: an experimental study, J. Adv. Res. Fluid Mech. Therm. Sci 12 (1) (2015) 1–10.
[46] G.R. Kefayati, Mixed convection of non-Newtonian nanofluids flows in a lid-driven enclosure with sinusoidal temperature profile using FDLBM, Powder Technol. 266 (2014) 268–281.
[47] M. Izadi, A. Behzadmehr, D. Jalali-Vahida, Numerical study of developing laminar forced convection of a nanofluid in an annulus, Int. J. Therm. Sci. 48 (11) (2009) 2119–2129.
[48] M. Izadi, A. Behzadmehr, M. Shahmardan, Effects of inclination angle on laminar mixed convection of a nanofluid flowing through an annulus, Chem. Eng. Commun. 202 (12) (2015) 1693–1702.
[49] M. Izadi, A. Behzadmehr, M.M. Shahmardan, Effects of discrete source-sink arrangements on mixed convection in a square cavity filled by nanofluid, Korean J. Chem. Eng. 31 (1) (2014) 12–19.
[50] M. Izadi, M. Shahmardan, A. Behzadmehr, Richardson number ratio effect on laminar mixed convection of a nanofluid flow in an annulus, Int. J. Comput. Methods Eng. Sci. Mech. 14 (4) (2013) 304–316.
[51] M. Izadi et al., Numerical study of developed laminar mixed convection of Al_2O_3/water nanofluid in an annulus, Chem. Eng. Commun. 200 (7) (2013) 878–894.
[52] O.A. Beg et al., Comparative numerical study of single-phase and two-phase models for bio-nanofluid transport phenomena, J. Mech. Med. Biol. 14 (01) (2014) 1450011.
[53] M. Rashidi et al., Comparative numerical study of single and two-phase models of nanofluid heat transfer in wavy channel, Appl. Math. Mech. 35 (7) (2014) 831–848.
[54] F. Garoosi et al., Numerical simulation of natural convection of the nanofluid in heat exchangers using a Buongiorno model, Appl. Math. Comput. 254 (2015) 183–203.
[55] L. Zhou, Y. Xuan, Q. Li, Multiscale simulation of flow and heat transfer of nanofluid with lattice Boltzmann method, Int. J. Multiph. Flow 36 (5) (2010) 364–374.
[56] Y.-T. Yang, F.-H. Lai, Numerical study of flow and heat transfer characteristics of alumina-water nanofluids in a microchannel using the lattice Boltzmann method, Int. Commun. Heat Mass Transfer 38 (5) (2011) 607–614.
[57] N.A.C. Sidik et al., Simulation of forced convection in a channel with nanofluid by the lattice Boltzmann method, Nanoscale Res. Lett. 8 (1) (2013) 178.
[58] V. Trisaksri, S. Wongwises, Critical review of heat transfer characteristics of nanofluids, Renew. Sustain. Energy Rev. 11 (3) (2007) 512–523.
[59] L. Godson et al., Enhancement of heat transfer using nanofluids—an overview, Renew. Sustain. Energy Rev. 14 (2) (2010) 629–641.
[60] Z. Haddad et al., A review on natural convective heat transfer of nanofluids, Renew. Sustain. Energy Rev. 16 (7) (2012) 5363–5378.
[61] A.M. Hussein et al., A review of forced convection heat transfer enhancement and hydrodynamic characteristics of a nanofluid, Renew. Sustain. Energy Rev. 29 (2014) 734–743.
[62] K. Khanafer, K. Vafai, M. Lightstone, Buoyancy-driven heat transfer enhancement in a two-dimensional enclosure utilizing nanofluids, Int. J. Heat Mass Transfer 46 (19) (2003) 3639–3653.
[63] H. Brinkman, The viscosity of concentrated suspensions and solutions, J. Chem. Phys. 20 (4) (1952), p. 571-571.
[64] H.E. Patel et al., A micro-convection model for thermal conductivity of nanofluids, International Heat Transfer Conference 13, Begel House Inc., 2006.
[65] P.L. Bhatnagar, E.P. Gross, M. Krook, A model for collision processes in gases. I. Small amplitude processes in charged and neutral one-component systems, Phys. Rev. 94 (3) (1954) 511.
[66] S.-L. Han, P. Zhu, Z.-Q. Lin, Two-dimensional interpolation-supplemented and Taylor-series expansion-based lattice Boltzmann method and its application, Commun. Nonlinear Sci. Numer. Simul. 12 (7) (2007) 1162–1171.
[67] Y. Peng, C. Shu, Y. Chew, Simplified thermal lattice Boltzmann model for incompressible thermal flows, Phys. Rev. E 68 (2) (2003) 026701.
[68] K. Han, Y. Feng, D. Owen, Modelling of thermal contact resistance within the framework of the thermal lattice Boltzmann method, Int. J. Therm. Sci. 47 (10) (2008) 1276–1283.
[69] C.-C. Chang, Y.-T. Yang, T.-H. Yen, Numerical investigation into thermal mixing efficiency in Y-shaped channel using Lattice Boltzmann method and field synergy principle, Int. J. Therm. Sci. 48 (11) (2009) 2092–2099.
[70] L. Zheng et al., Lattice Boltzmann equation for axisymmetric thermal flows, Comput. Fluids 39 (6) (2010) 945–952.
[71] C.N. Azwadi et al., Numerical prediction of free convection in an open ended enclosure using lattice Boltzmann numerical method, Int. J. Mech. Mater. Eng. 8 (2013) 58–62.
[72] J. Wang et al., Lattice Boltzmann simulations of thermal convective flows in two dimensions, Comput. Math. Appl. 65 (2) (2013) 262–286.
[73] A.A. Mohamad, Lattice Boltzmann Method: Fundamentals and Engineering Applications with Computer Codes, Springer Science & Business Media, 2011.
[74] Y. Yan, Y. Zu, Numerical simulation of heat transfer and fluid flow past a rotating isothermal cylinder – a LBM approach, Int. J. Heat Mass Transfer 51 (9) (2008) 2519–2536.
[75] A. Mohamad, Applied lattice Boltzmann method for transport phenomena, momentum, heat and mass transfer, Can. J. Chem. Eng. 85 (6) (2007), p. 946-946.
[76] J. Wang, M. Wang, Z. Li, A lattice Boltzmann algorithm for fluid–solid conjugate heat transfer. The present work was supported by the National Natural Science Foundation of China (Grant No. 59995550–2), Int. J. Therm. Sci. 46 (3) (2007) 228–234.

[77] L. Jahanshaloo et al., An overview of boundary implementation in lattice Boltzmann method for computational heat and mass transfer, Int. Commun. Heat Mass Transfer 78 (2016) 1–12.
[78] S. He, B.T. Habte, F. Jiang, LBM prediction of effective thermal conductivity of lithium-ion battery graphite anode, Int. Commun. Heat Mass Transfer 82 (2017) 1–8.
[79] N. Janzadeh, M. Aghajani Delavar, Using lattice Boltzmann method to investigate the effects of porous media on heat transfer from solid block inside a channel, Transp. Phenom. Nano Micro Scales 1 (2) (2013) 117–123.
[80] Q. Zou, X. He, On pressure and velocity boundary conditions for the lattice Boltzmann BGK model, Phys. Fluids 9 (6) (1997) 1591–1598.
[81] T. Inamuro, M. Yoshino, F. Ogino, A non-slip boundary condition for lattice Boltzmann simulations, Phys. Fluids 7 (12) (1995) 2928–2930.
[82] R. Mei, L.-S. Luo, W. Shyy, An accurate curved boundary treatment in the lattice Boltzmann method, J. Comput. Phys. 155 (2) (1999) 307–330.
[83] R.K. Shah, A.L. London, Laminar Flow Forced Convection in Ducts: A Source Book for Compact Heat Exchanger Analytical Data, Academic Press, 2014.
[84] F. Durst, Fluid Mechanics: An Introduction to the Theory of Fluid Flows, Springer Science & Business Media, 2008.
[85] D.F. Elger, J.A. Roberson, Engineering Fluid Mechanics, Wiley, Hoboken (NJ), 2013.
[86] G. Tang, W. Tao, Y. He, Simulation of fluid flow and heat transfer in a plane channel using the lattice Boltzmann method, Int. J. Mod. Phys. B 17 (01n02) (2003) 183–187.
[87] H. Heidary, M. Kermani, Heat transfer enhancement in a channel with block (s) effect and utilizing Nano-fluid, Int. J. Therm. Sci. 57 (2012) 163–171.